

Dynamics of pore fouling by colloidal particles at the particle level

B. Dersoir, A. B. Schofield, Matthieu Robert de Saint Vincent, Hervé Tabuteau

▶ **To cite this version:**

B. Dersoir, A. B. Schofield, Matthieu Robert de Saint Vincent, Hervé Tabuteau. Dynamics of pore fouling by colloidal particles at the particle level. Journal of Membrane Science, 2019, 573, pp.411-424. 10.1016/j.memsci.2018.12.025 . hal-01996695

HAL Id: hal-01996695

https://univ-rennes.hal.science/hal-01996695

Submitted on 27 Aug 2020

HAL is a multi-disciplinary open access archive for the deposit and dissemination of scientific research documents, whether they are published or not. The documents may come from teaching and research institutions in France or abroad, or from public or private research centers.

L'archive ouverte pluridisciplinaire **HAL**, est destinée au dépôt et à la diffusion de documents scientifiques de niveau recherche, publiés ou non, émanant des établissements d'enseignement et de recherche français ou étrangers, des laboratoires publics ou privés.

ACCEPTED MANUSCRIPT

Dynamics of pore fouling by colloidal particles at the particle level B. Dersoir[a], A.B. Schofield[b], M. Robert de Saint Vincent[a], H. Tabuteau[a]*

a Univ Rennes, CNRS, IPR (Institut de Physique de Rennes)-UMR 6251, F-35000 Rennes, France

b School of Physics and Astronomy, The University of Edinburgh, The James ClerkMaxwell Building, The King's Buildings, Mayfield Road, Edinburgh, UK

Abstract

Particle filtration occurs whenever particles flow through porous media such as membrane. Progressive capture or deposition of particles inside porous structure often leads to complete, and generally unwanted, fouling of the pores. Previously there has been no experimental work that has determined the particle dynamics of such a process at the pore level, since imaging the particles individually within the pores remains a challenge. Here, we overcome this issue by flowing fluorescently dyed particles through a model membrane, a microfluidic filter, imaged by a confocal microscope. This setup allows us to determine the temporal evolution of pore fouling at the particle level, from the first captured particle up to complete blocking of the pore. We show that from the very beginning of pore fouling the immobile particles inside the pore significantly participate in the capture of other flowing particles. For the first time it is determined how particles deposit inside the pore and form aggregates that eventually merge and block the pore.

Introduction

Fouling by colloidal particles remains a major issue in many industrial processes including particle synthesis and solid handling in microreactors, membrane filtration, and liquid chromatography, often leading to complete stoppage of the process [1]. Even though this clogging issue is specific to each application, some generic features have been identified thanks to the use of microfluidic technology coupled with various imaging techniques such as confocal microscopy [2–7]. This technology enables the design of microdevices with complex geometries [8] that mimic industrial processes, in particular membrane filtration, and inside these devices we can follow the capture or deposition of colloidal particles over time, at the pore scale level, using diverse microscopy techniques. The main parameters that control the fouling behavior at the pore level have been isolated and studied over the last decade thanks to the microfluidic approach. Studies have determined the influence of pore geometry (width, shape, length, varying or fixed cross section) [3,5,9–11], the confinement, i.e. the ratio between the particle radii and the smallest dimension of the pore [4,5,10], the polydispersity of the colloidal suspensions [12,13], the stability of the suspension with respect to the DLVO interaction potentials, between particles and the pore walls and between particles themselves [3–5,14–16], and the deformability of the particles [6].

Despite these efforts to visualize the fouling process inside model membranes, the dynamics inside a pore at the particle level remain completely unexplored. Almost all the work that has used either microfluidic setups or various kinds of membranes or microsieves onlyfocus on pores that are already partially or completely clogged, thereby ignoring the particle deposition history [3,6,17–20].

Accepted manuscript

In more complex situations where solids are continuously formed inside a tube, due to a chemical reaction, several studies have provided some information on aggregate growth that ends up blocking the pore [21–23]. In particular, Sicignano et al. [22] have shown that the shape of solid aggregates of potassium bromide that deposit on the pore walls of the reactor during a chemical reaction strongly depends on the flow conditions. At low flow rates the aggregates formed are rather fractal while at higher flow rates they are more compact. These aggregate morphologies and porosities have a direct impact on the clogging properties. However, even though the authors provide confocal images of the clog, its local structure (particle coordination number, local porosity) remains completely undetermined.

In most cases, fouling dynamics remain accessible almost only by the macroscopic measurement of pressure or flux decline as particles get captured inside the pores or on top of membranes. In a more local investigation, Warkiani et al. provided images of the progressive fouling of a given zone of a membrane [18]. However these images do not allow us to quantify important features of membrane fouling such as the rate of particle deposition over time or the degree of fouling, i.e., the remaining pore space, which would shed a structural light on the local hydrodynamics. Up to now, the critical number of particles required to clog a pore for a given set of suspension (e.g., DLVO parameters) and membrane (e.g., geometry) properties remains unknown. In a recent publication [8], we have considered the clogging dynamics at the particle level for various flow conditions in very confined situations where the pore height H is only slightly larger than the particle diameter D ($1.2 < H/D < 1.75$), the pore width being very large compared to its height ($W/H > 20$). In such a slotted pore geometry we showed that there are two regimes of fouling. At low flow rates pore clogging is only due to the particle capture by the pore walls at the very entrance of the pore. At higher flow rates a few isolated particles are also captured within the pore. Hydrodynamic interactions between these immobile particles and those flowing are now mainly responsible for the subsequent particle deposition on the pore walls. This particular capture mechanism leads to the growth of bi-dimensional aggregates that quickly obstruct the pore.

In the present study we would like to investigate the clogging dynamics, still at the particle level, to thicker pores featuring a nearly square cross section (height $H=3D$ and width $W=4D$). In such conditions the pore cannot be clogged only by particle deposition on the pore walls. There must be particle capture on top of a first layer of particles that is already in contact with the pore walls to block the pore. In the first section of this manuscript we examine fouling at the pore level for various conditions (hydrodynamics, confinement and physical-chemistry). Thereafter we examine fouling at the pore level from the first captured particle up to the complete blocking of the pore. Confocal microscopy gives us access to the position of the individual particles inside the pore as they get captured, allowing us to determine the particle deposition curve throughout the fouling process. We thus characterize, in a second section, all the capture mechanisms that lead to pore fouling, which includes direct capture by the pore, indirect capture due to particle-particle hydrodynamic interactions, and bulk deposition on top of other immobile particles. Thereafter, we determine

Accepted manuscript

ACCEPTED MANUSCRIPT

how aggregates grow within the pore and eventually block it, and finally we discuss our results in a broader perspective.

1- Experimental

1-1 Colloidal particles and microfluidic setup

We have synthesized 4.1 µm diameter PMMA (polymethylmetacrylate) particles following the method developed by Shen et al. [24]. These particles are monodisperse (CV=2.5%) and are dyed with NBD (4 chloro-7-nitrobenz-2 oxa-1,3 diazole) which is excited at 488 nm and has a maximum in emission at 525 nm. Polyvinylpyrrolidone (PVP) chains that bear negative charges stabilize them against aggregation in aqueous suspension. The resulting zeta potential and the Critical Coagulation Concentration (CCC) are equal to -70mV and 0.35M respectively.

For each experiment we pipette a few tens of microliters of the mother PMMA suspension (10% by weight in Millipore water) and add it to a suspending liquid composed of water (33% by weight), urea (37%) and glycerol (30%) to get very dilute suspensions (particle volume fraction in the order of 10^{-5}). This composition was chosen to minimize both the density and refractive index mismatches between the particles and the suspending liquid. The final suspension is shaken by hands and sonicated for half an hour to break the residual colloidal aggregates. In our experiments we flow these dilute suspensions through a microfluidic device that acts as a particle filter (Figure 1A). The filter part consists of a series of parallel pores of width W=16µm, corresponding to 4D, D being the particle diameter (figure 1B). Upstream of each pore there is a reservoir zone, which is three times wider than the pore. Experiments are stopped before these reservoir zones get full of particles to ensure that there is no cross-talk between adjacent pores and that the variation of the flux within a given pore is only due to the particle deposited inside this pore. Therefore this local flux decline in each pore is not influenced by the progressive or complete clogging of its neighbors [4]. The microfluidic device is made of PDMS (polydimethylsiloxane) following the standard soft lithography protocol [25]. We made the device using a negative photoresist (SU8 2010) with a height H of 12µm corresponding to three particle diameters. PDMS is then poured on the photoresist, cured, punched to create the inlet and outlet, and sealed onto a PDMS coated glass cover slip which enables imaging inside the pore with an X63 oil immersion objective (NA =). Flow through the microchannel is imposed at constant pressure gradient across the microchannel, thanks to precise pressure controllers (Elveflow MK2 or Fluigent MFCS). Colloidal particles first flow in the main channel and then in one of the parallel pores (Figure 1A-C). The flow condition within each pore are thus kept constant, by applying a pressure drop ΔP=30 mbar, within the pressure range in which the number of particles that have to flow through the pore prior to clogging is fixed [5]. Actually the experiment is stopped when five pores are clogged, which leads to a small variation of the total flow rate ($Q_{final} = 0.8Q$, with Q the total flow rate at the beginning of the experiment). During a typical experiment, we study the progressive clogging of nine parallel pores. The Re number is always smaller than 10^{-4} and the Pe number is between 10 and 100. We worked with an isodense suspension, i.e. the

Accepted manuscript

ACCEPTED MANUSCRIPT

density of the liquid and the colloidal particles are the same. In summary, the effects of inertia, Brownian diffusion, and sedimentation can be neglected.

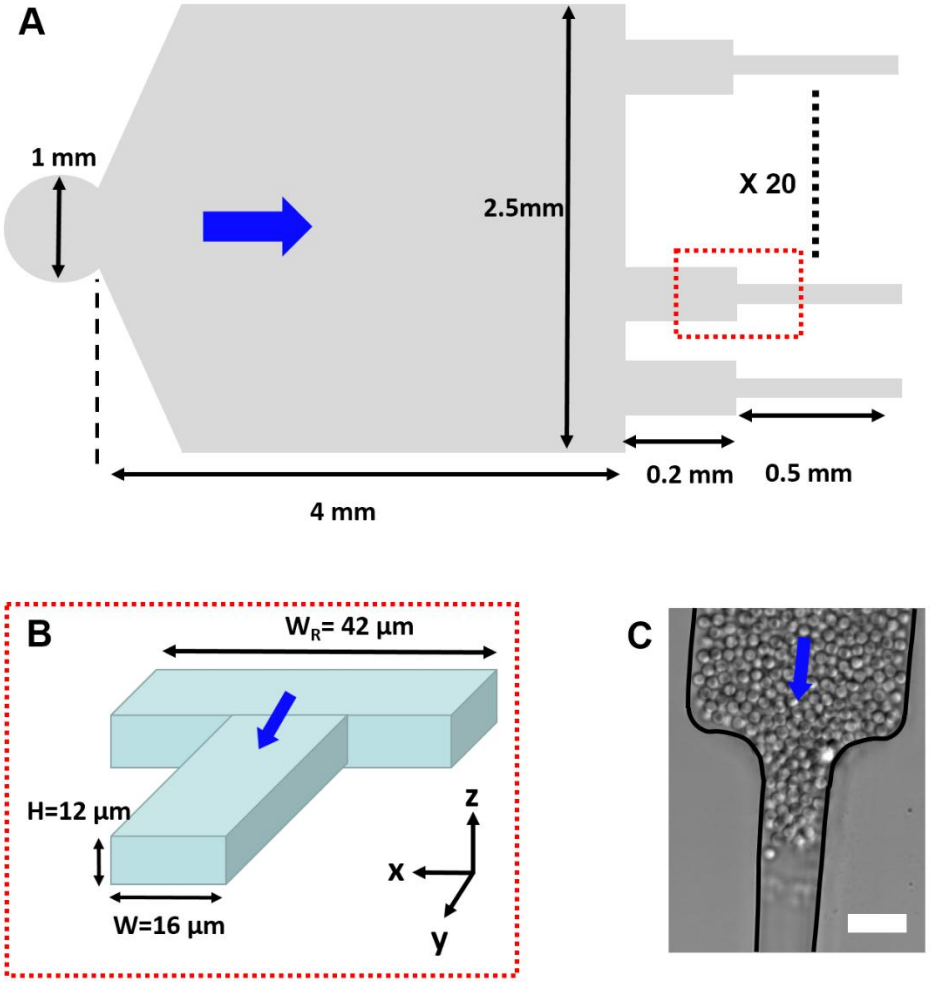


Figure 1: A-Geometry of the microfluidic model filter. B-Close-up view of the reservoir and the pore entrance zones. C-Top view image of a clogged pore. The black lines correspond to the outlines of the pore. The blue arrows point to the flow direction. The scale bar corresponds to 16µm.

Accepted

1-2 Image acquisition and analysis

We used a confocal microscope (VT-Infinity III, Visitech) to image the particles within the pore. During this process we perform a z-stack along the pore height which is composed of 40 positions taken every 0.5µm with a piezometer z-stage. This z-stack for each pore is performed in 2s. In this way we get 8 xy plans or section per particles. These conditions are sufficient to determine precisely the particle center and to achieve a reliable identification of the particles we used the algorithm developed by Crocker and Grier [26].

This algorithm uses the fact that particles are spheres to find their centroid coordinates and identifies the local maxima in the intensity profile of each particle. We will first describe this method applied to a 2 dimensional image and then generalized to a 3 dimensional confocal stack of images. The calculation of the image of a spherical colloid, i.e. its intensity profile, given by fluorescence or confocal microscopy, is still a real theoretical challenge, but it can be roughly thought as a Gaussian surface of revolution as suggested by

ACCEPTED MANUSCRIPT

Crocker and Grier [26]. We assume that the ideal image of a particle is thus a Gaussian blob. The real image obtained with a microscope is naturally not this ideal image and it suffers from inherent noise and distortions primarily coming from the camera and also, to a lesser extent the optics of the microscope (figure 2A). The first step in the analysis used to identify the center of the particles is to clean the image. Applying a spatial band-pass filter smooths the image and subtracts the background. Uneven illumination and non-uniformity among the camera's pixels often causes contrast gradients in the image and long wavelength modulation in the background brightness.

For typical images of a suspension of colloidal particles, which are not too concentrated, i.e., particles are well separated from each other, the background can be determined simply by averaging the intensity over a region defined as larger than twice the radius of a single sphere but smaller than inter-sphere separation. A background image can be then obtained by a convolution of a boxcar average over the defined region. Short wavelength modulations are due to the noise created by the camera. Such noise is purely random and has a short correlation length of about a pixel. A convolution of the image with a Gaussian surface of revolution of half width 1/2 pixel (Gaussian blurring) allows to get rid of this noise. We apply both these convolutions to the images to perform the band-pass filtering. The difference between the noise-reduced and background images gives us an image close to the ideal Gaussian one. After this filtering, each particle should become a single rounded peak, the local maximum corresponding to the center of the particle. Figure 2B and C shows the effect of the band-pass filtering and the corresponding intensity profile for an assembly of particles.

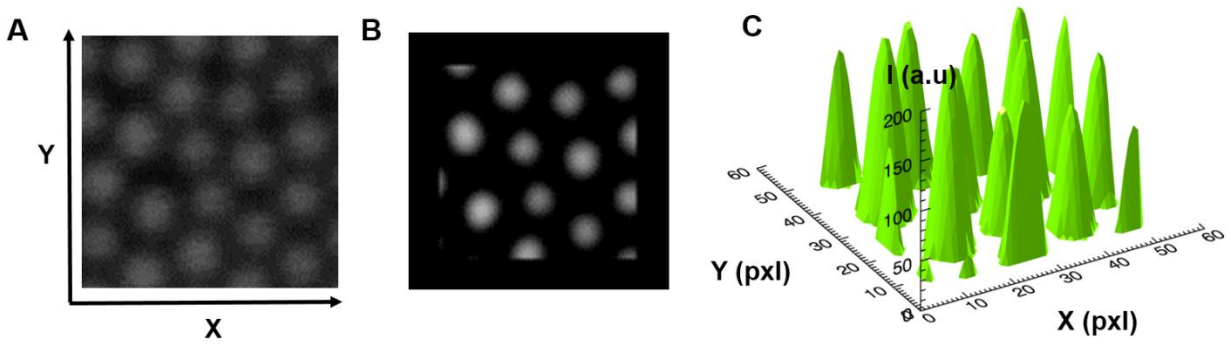


Figure 2: A-Raw confocal image of spherical colloids. B-The image in A after a spatial band pass filtration. C-Intensity surface plot of the image B.

Once the image is filtered, the next step is to extract the possible particle positions. Assuming that the image of a particle has a maximum intensity at its center, we identify candidate particle locations as the local brightness maxima within the image. We search the pixels that have no brighter neighbors at a distance corresponding to one particle diameter. This step provides an estimate of the particle location with nearest pixel accuracy.

Another refinement is necessary to obtain a sub-pixel accuracy. To do so we use the fact that our colloidal particles have a spherical shape, regardless of the fluorescence intensity profile. We can thus use this symmetry to refine the position of the particle using a brightness-weighted centroid. Identifying the center of

ACCEPTED MANUSCRIPT

mass of the intensity profile of the pixel surrounding the possible center results in a precision in location around 30-40nm in the image plane.

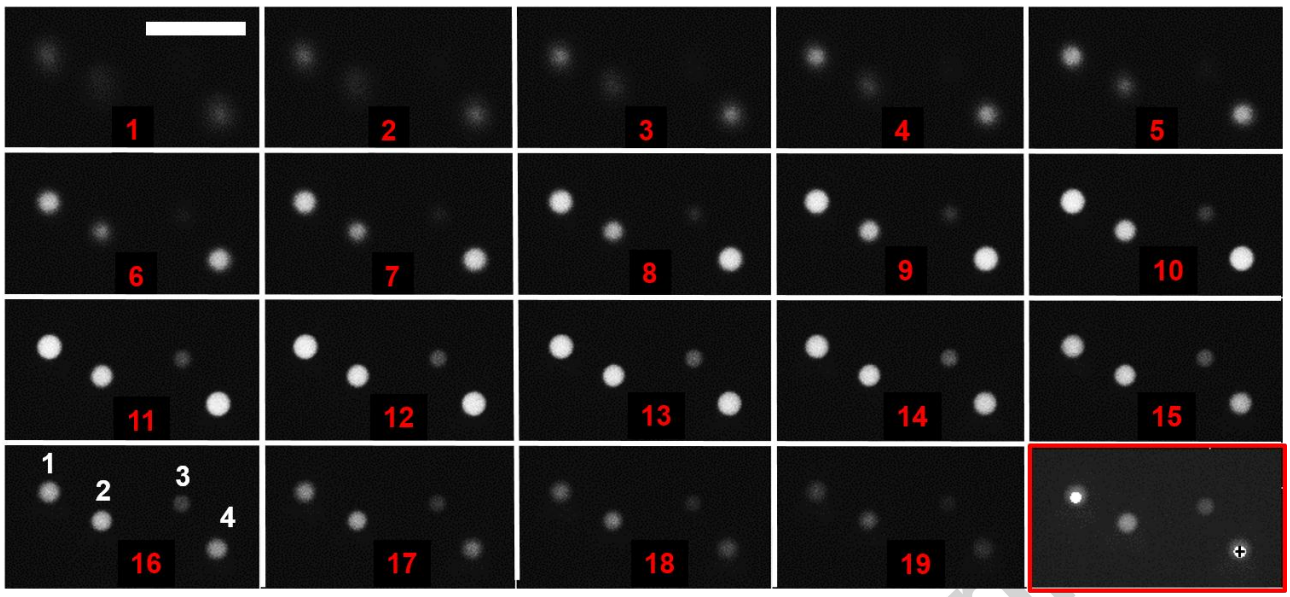


Figure 3: z-stack of 19 confocal images. Consecutive images are separated by a vertical distance of 0.5µm. There are four particles inside the volume, spotted in image 16. The location of the center of the 4th particle along the z direction corresponds to the z-plane obtained in image 16. The black cross within this particle in the bottom right corner image correspond to the position of the center of the 4th particle in the x-y plane. The white scale bar corresponds to 16µm.

We can also retrieve the three dimensional coordinates in a confocal z-stack. A z-stacks consists in imaging the sample at different focal planes, as typically illustrated in Figure 3. On each image of the z-stack, we perform the 2d tracking algorithm and while looping over the particles we calculate centroid refinements, the moments ??0 and ??2 of each candidate image's brightness. In a given frame of the z-stack, particles form a roughly elliptical cluster in the (??0, ??2) plane. For each particle, we collect the probability distribution ??(???? |??0, ??2) for the center of a particle to be within ???? of ???? given its moments ??0 and ??2. Summing this probability function for each frame in the z-stack allows an estimation of the particle's vertical position (figure 3, bottom right corner). This method finds the z coordinate of the particle with an error that is ten times larger than the location of the particle center in the x-y plane.

Centroid refinement is the most widely used refinement technique for particle location determination. However, even though it is successful in most scenarios, the precision of particle center location is not optimal and in particular this is the case for, particles whose size is close to the resolution of the imaging apparatus such as for micron sized colloids. There are also problems when particles are close together so that their particle spread functions overlap. Since in this article we work with particles that are in contact within a clog, we need to use another refinement method to overcome the issues of the centroid method. We choose the Sphere Spread Function (SSF) refinement method developed by Jenkins and Egelhaaf [27]. The image of a colloidal particle given by the microscope is the convolution of the sphere response to the illumination light (or emission for fluorescent particles) with the microscope's point spread function, and the resulting

Accepted manuscript

ACCEPTED MANUSCRIPT

pattern is called the sphere spread function (SSF) as defined by Jenkins and Egelhaaf [27]. Like the centroid method, the SSF refinement relies on a priori knowledge of the SSF. When imaging immobile or slowly moving particles (which is our case) we can reconstruct an experimental SSF by averaging over the image of each particle. This experimental SSF allows us to account properly for experiment dependent imperfections such as index mismatch. After determining the experimental SSF, we can refine the particle position by searching for the location that best matches the SSF within a window around its original coordinates. We compare every pixel value in the SSF to every value in the image window to form a chi-square hypersurface. This ??² presents a minimum at the particle's location that can be found with sub-pixel accuracy by determining the minimum in the three directions and interpolating for a large number of points lying within half a pixel around the minimum of ??². We used this method to locate immobile particles, captured inside the pore.

The determination at the particle level of the features of the progressive fouling also requires some specific conditions with respect to the difference of refractive index of the particles with that of the suspending liquid. If this difference is too large, typically higher than 0.1-0.2, we cannot image properly more than one layer of particles inside the pore.

This was the case when we studied pore clogging with polystyrene particles dispersed in water within microchannels [5,28]. Indeed, for such a difference there is multiple light scattering from the first monolayer of particles on the bottom horizontal part of the pore, which is in contact with the coated cover slip. This light scattering prevents the visualization of the particles located above this monolayer and even with a confocal microscope these particles remain fuzzy and no qualitative analysis of their position is possible.

Here we work with a suspending liquid that has a refractive index of 1.42. In this case the difference between the refractive index of the particles (1.48) and that of the suspending liquid is equal to 0.06, which allows us to image perfectly all the particles layers across the pore height (figure 4). From the images we can thus reconstruct the structure of the deposit, starting from the first particles captured by the pore wall (figure 4A) up to complete blocking (figure 4D).

The number of particles that flow through a pore over time can be adjusted through the volume fraction of the suspension. We choose it in a way that, on average, about one particle deposits in each pore every 30s, a rate sufficiently slow to allow us imaging several pores in parallel yet still recording about all particle capture events. Since we have no image acquisition rate limitations we could have monitored the clogging process for only one pore per microfluidic device at a time and then repeat this for another pore. However we faced two issues in doing this. Firstly we would have to decide which pore to follow and this could have been one of the last pores of the microfluidic device to be clogged. In this circumstance the clogging dynamics could be a bit slower and the structuration of the deposit may also be different, due to the change of the average flow rate inside the device. Secondly, even though the suspension is rather monodisperse, there are always big particles within it in a minute concentration. We often observed a few depositions of 4µm particles inside the pore and then 8 to 14µm ones appear that block its entrance. Since our aim is to study pore clogging by aggregation and not by sieving, we try to avoid this situation. We then decided to

Accepted manuscript

ACCEPTED MANUSCRIPT

image several pores at the same time and choose at the end of the experiment those which were clogged first and also did not contain any big particles.

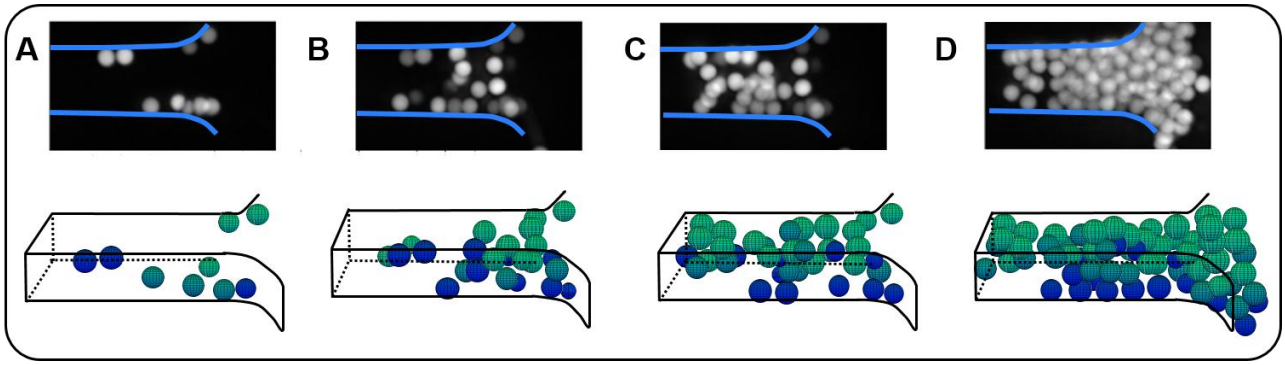


Figure 4 : A-D Confocal image of a pore progressively fouled by the deposition of colloidal particles. (top) Z-Projection (projection on one plan) of all the images taken during a z-stack of a pore. (Bottom) Corresponding reconstruction, after image analysis, of the deposit. Particles are depicted according to a blue-green color gradient representative of their vertical position (dark blue: particle on the floor; green: particle on the roof). The flow goes towards the left.

Results

1-1 Clogging at the pore scale: influence of the flow conditions and the ionic strength

In a previous study we determined the clogging mechanisms of single and squared cross section pores by polystyrene (PS) particles (diameter between 1 and 10µm) [5]. We performed systematic experiments using several degrees of confinement (ratio of the pore width *W* over the particle diameter *D*), between 1.5 and 10, and under different flow conditions. We also work with isodense suspensions where the density of the fluid and the particles are the same, by using mixture of water and heavy water. We defined the average clogging dynamics with the help of the variable *N**, which is the total number of particles that had flowed through the pore prior clogging. We also determined the length of the clog from the pore entrance L_{clog}. Since in this study we use a different type of particle, these made of PMMA, we have performed systematic experiments at the pore scale to determine the evolution of *N** and L_{clog} under various flow conditions, degrees of confinement (*W/D*=3.5, 4.5 and 6) and with two ionic strengths. We have provided additional experiments for PS particle with a high ionic strength of 0.05*M* that is just below the Critical Coagulation Concentration (CCC= 0.07*M*).

Whatever the type of particles, PS or PMMA, we found the same behavior, i.e., there are three clogging regimes depending on the flow conditions (Figure 5) [5]. In the first regime, *N** and L_{clog} remain constant over a decade in pressure. It is worth noting that the values of L_{clog} do (almost) not depend on the ionic strength for a given ratio *W/D*. L_{clog} is around 1.4W for the PS particles, and close to 2.6W for the PMMA ones (Figure 5a-b). In contrast, we found that the value of *N** strongly depends on the ionic strength *I*. Adding salt to the suspension indeed screens the electrostatic interactions, which essentially leads to a faster clogging dynamics, keeping almost the same geometrical features of the clog in both regimes. For PMMA colloids, when *I* rises from 0.05 up to 0.15M there is a decrease of *N** by a factor of 2.5 (Figure 5d). Besides,

Accepted manuscript

ACCEPTED MANUSCRIPT

note that the value of N^* is roughly three orders of magnitude higher for PMMA than for PS (Figure 5c-d). The capture probability of PMMA particles is then considerably lower than that of the PS ones. This is directly related to the difference in surface charge between the two types of particle. In addition, since the PMMA particles have a lower adhesion on the PDMS walls than the PS ones, the first clogging regime occurs over a much shorter range of pressure for the PMMA particles, i.e., lower applied pressure is needed to detach particles from the pore walls [5]. In the second regime, observed at higher pressures, L_{clog} starts to rise up and declines progressively toward a value smaller than that of the first regime. At the same time, N^* also increases with the pressure, and levels off thereafter for all the suspensions, at a value higher than in the previous regime. In this regime the flow is able to detach particles from pore walls, especially where the intensity of the flow in the strongest. Finally, for the highest pressures, in a third regime, pores are not clogged anymore even though there are some particles deposited on the pore surface. The shear flow is so strong near the pore surface that it erodes instantaneously the particles which may stick onto this first layer of particles.

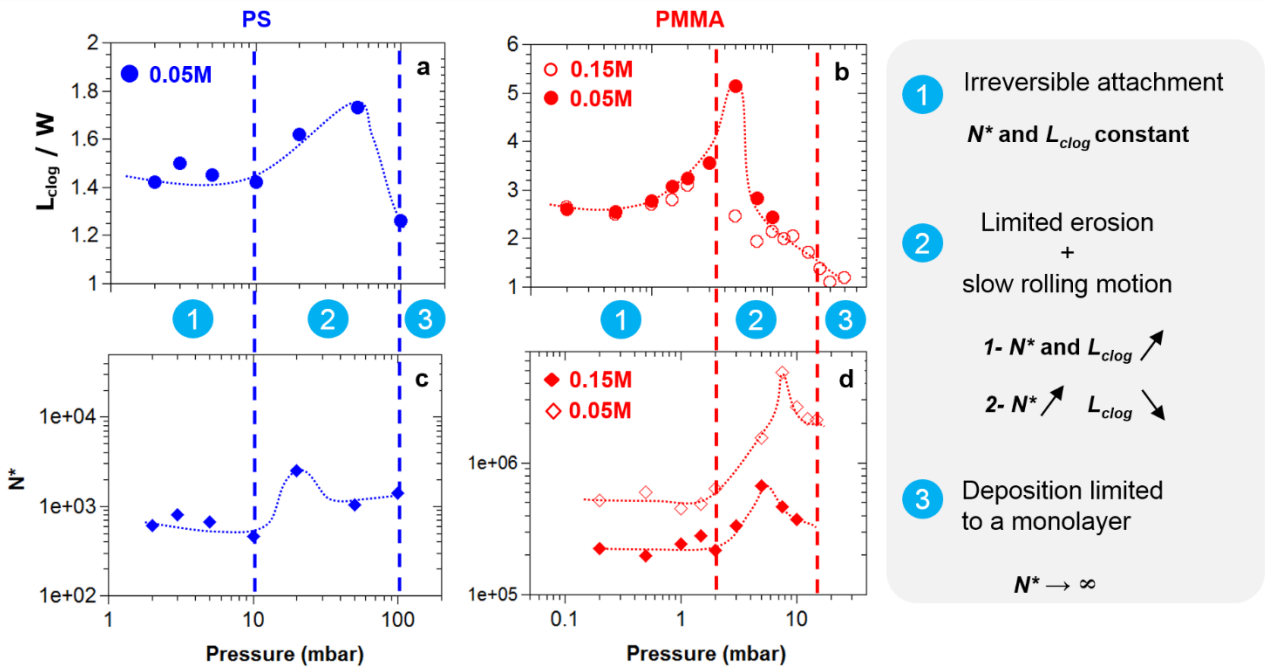


Figure 5: Evolution of N^* and L_{clog} with the applied pressure difference, for 2µm PS and 4µm PMMA particles inside a pore with a width equals to 8 and 18 µm respectively. The dashed lines correspond to the transition between the three clogging regimes. The main features of each regime are summarized on the right panel.

The influence of three coupled phenomena is responsible for the variation of N^* and L_{clog} in the first two regimes. To begin with, the shadow effect could explain the first increase of L_{clog}. Indeed, the size of the excluded zone of capture, just upstream of a deposited particle increases with the average flow rate (the applied pressure). Moreover this blocked area is not symmetric with respect to the direction of flow. The blocked area is larger downstream of the particle than upstream [29,30]. Therefore, the distance between particles within the first layer is greater which might result in a broadening of L_{clog}. Secondly, we observed that the number of particles deposited on the pore surface decreases as the pressure increases in the second

ACCEPTED MANUSCRIPT

regime. This reduces the probability of capture upon the first layer, implying an increase of N^* as observed. Finally, we have observed that PMMA particles can move slowly (in the order of 0.1µm/s) after they are captured on the pore surface. The shear flow induces this rolling motion of the particles because the attractive part of the particle wall potential is shallow for this type of particles. This tendency is enhanced as the pressure and the ionic strength increase. We expect that the same effect occur for the PS as well, but in a lesser extent. We indeed observed particles motion with a high speed camera but we do not have enough statistics to get an average velocity out of it.

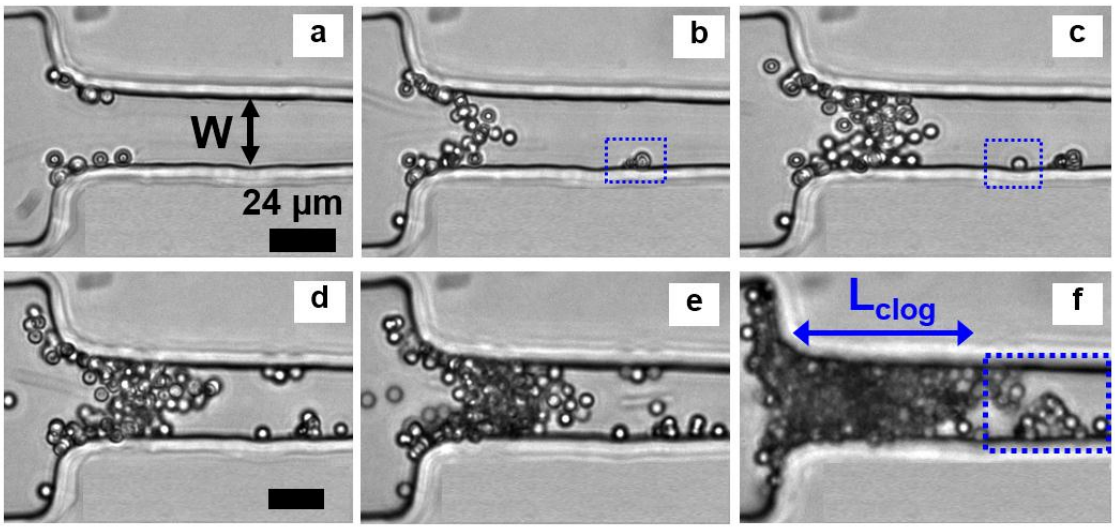


Figure 6: Images of the clog building-up by 4 µm PMMA particles inside a pore of width W and height H both equal to 24µm. At the end of the clogging (image f), the isolated aggregate (highlighted by the dotted rectangle) does not partake to the growth of the main clog. L_{clog} is equals to 2.8W.

In the following we focus on the first regime in which N^* and L_{clog} remain constant with the applied pressure. A typical progressive fouling of a pore by PMMA particles in bright field microscopy is shown in Figure 6. The particles first deposit on the lateral pore walls (image a) and then get captured on the bottom and the top walls (image b-c). Right from the beginning of the experiment new captured particles get deposited near immobile one (image a and b). However, isolated particles may deposit further downstream inside the pore due either to the presence of dust (rectangles in image b) or an imperfection of the pore wall (rectangles in image c). Aggregates grow up at these places (rectangle in image f) until the end of the clogging process, independently of the main clog that develops at the pore entrance. From the bright field images for all the degrees of confinement we can observe the same trend: the growth of few aggregates is responsible of the pore clogging, at least at the beginning of the experiments. However quite rapidly we cannot quantify this growth since we are unable to distinguish individual particles on the images. Thereafter we focus on the degree of confinement W/D~3.5 since under these conditions we can determine with a high accuracy the position of the particles within the pore by using the confocal microscope. We choose a pressure of 30 mbar, a value which is well below the pressure needed to detach particles from the wall. In such conditions the dynamics of pore clogging at the particle level is not identical to that observed in our previous paper where the confinement was quite high ($1.2< H/D < 1.75$) [10]. The shape of the pore is not the same as well: a nearly square cross section pore is used in this work while a slit pore with a width much greater than its

ACCEPTED MANUSCRIPT

height was used in the former publication [10]. The capture mechanism of the particles by the pore walls, thereafter called *direct capture*, are obviously the same in both works. However, the other particle capture mechanisms are different. In the more confined situation a flowing particle get captured thanks to an immobile one through a sieving process where the particle is trapped between an immobile particle and one of the two horizontal pore walls (cf. Figure.8 of [10]). In the present study, sieving by deposited particles is effective only at the very end of the clogging process. Here we show that the first particles deposited in the square pore also greatly help flowing particles to be captured, but following a different capture mechanisms to the sieving case. In addition the growth rate, the way aggregates spread inside the pore, and the stability of the particles attached to the pore walls are completely different in both works as we will see hereafter.

1-Building up of a clog: from the pore to the particle scale

We present in Figure 7 the progressive building-up of a clog at the particle level, corresponding to the particle deposition curve of Figure 8A. Particles first deposit at the pore entrance, mostly close to the corners (images 1 to 3). The capture of these particles is due to a physical interception of the particles by the pore surface as they enter into the pore [8]. Particles come close enough to the pore surface and fall into the attractive part of the interaction potential (DVLO) between the particle and the pore surface. In this example several particles then get captured further downstream within the pore (images 4 to 9). This later type of deposition results from either the presence of an impurity at the surface of the pore or a local imperfection of the pore surface (i.e. a bump or a valley coming from the fabrication of the microchannels), as shown in Figure 6, that facilitates particle capture. Note that we have only observed a couple of these 'fortuitous' particle depositions in all our experiments. Due to their rareness we were not able to characterize them properly but we assume that they have a limited influence on the overall fouling process, especially when these defects are far from the pore entrance. From N=9500 (image 7), particles start to be captured by other individuals, i.e., the deposition involves interparticle interaction rather than only particle-surface ones (yellow arrow in image 8). Thereafter few particles deposit on the second layer, i.e., on top of others while most of them still accumulate directly on the pore surface, especially on the bottom part of the pore (image 8 and 9). Finally, the pore gets completely clogged at its entrance. At this location the size of the remaining part of the pore is smaller than a particle size and then particles coming towards the pore entrance just pile up and form a cake in the reservoir zone upstream of the pore.

We also determined the clogging dynamics at the pore scale with the help of deposition curves. Figure 8 reports the evolution of the number of particles deposited inside the pore as a function of the number of particles that have flowed through the pore (N) for several pores. The respective clog structures at the end of the fouling process are given in the bottom part of Figure 7. In all cases we clearly see that the clogging dynamics can be decomposed into two steps. The number of particles deposited first increases slowly. In this step, a monolayer of particles is formed on all pore walls. Thereafter, the second step starts with the capture of a particle by another that has already been deposited. This feature is quite robust and thus observed in the three other examples (Figure 8B to D). During this second step particles can either participate in the formation of the second layer or keep depositing directly on the pore wall, ending up by completely blocking the pore. The average deposition rate is faster than in the first step. From all curves we clearly see that the

Accepted manuscript

ACCEPTED MANUSCRIPT

number of particles involved in each deposition step are not the same. This variability is inherent to the particle deposition process and the way successive particle capture occurs.

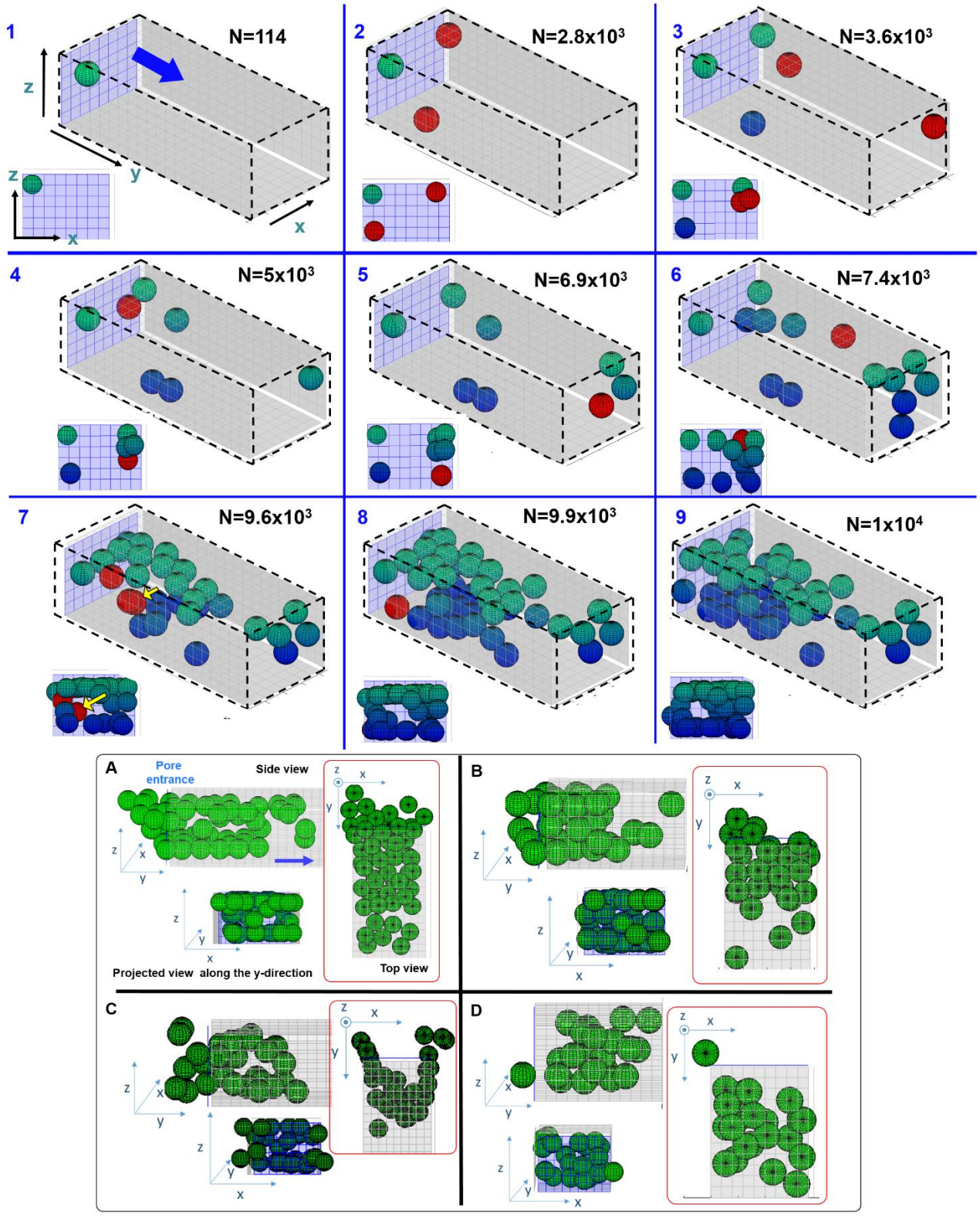


Figure 7: (Top) 3d images depicting the building-up of the clog. The blue plane represents the cross section at the entrance, and the grey ones the four pore walls. The blue arrow points to the flow direction. The red particles are the freshly captured ones. Particles are depicted according to a blue-green color gradient representative of their vertical position (dark blue: particle on the floor; green:

ACCEPTED MANUSCRIPT

particle on the roof). The projected view, perpendicular to the flow directions helps visualizing the progressive inward fouling. In image 7 the yellow arrow points towards the first particle that gets captured in bulk by immobile particles and not by the surface of the pore. (Bottom) Various 3D views of the clogs obtained at the end of the fouling process for the four trials. The views in top left corner corresponds to the final structure of the clog formation shown in the top part.

Indeed, although the particle capture may result from universal mechanisms, particles are not captured at the same location in each pore. For instance, at the very beginning of the clogging process, the first deposition events often occur in the corners (Figure 9). However the positions of those particles from the pore entrance are well distributed and can spread over a distance of up to 4.5 particle diameters (Figure 9D). These differences in the particle capture location will in turn affect the subsequent particles deposition in a different way. Indeed, looking at the final structure of each clog (Figure 7, bottom), we observe that there are more particles involved in the fouling process when the particle monolayer deposited on the pore walls extends further downstream from the pore entrance. The variability in particle capture scenarios therefore likely explains the variability in the dynamics observed for the different pores in Figure 7.

The number of deposited particles inside the pore varies roughly linearly with N during both the first and second steps, giving a constant rate of particle deposition for each step, i.e., the corresponding mean probability of particle deposition. This probability is between $2.2\text{x}10^{-3}$ and $6.8\text{x}10^{-3}$ in the first step (green dashed line) while it is between $1.4\text{x}10^{-2}$ and $4.8\text{x}10^{-2}$ in the second (red dashed line), thus seven times greater in the second step. Again the variation of the slopes from one pore to another in each step is due to the different spatial position of the particles inside each pore. There are rising-up parts followed by inactivity periods, during which no particle get captured. More rarely we observed single particle detachment events.

Accepted manuscript

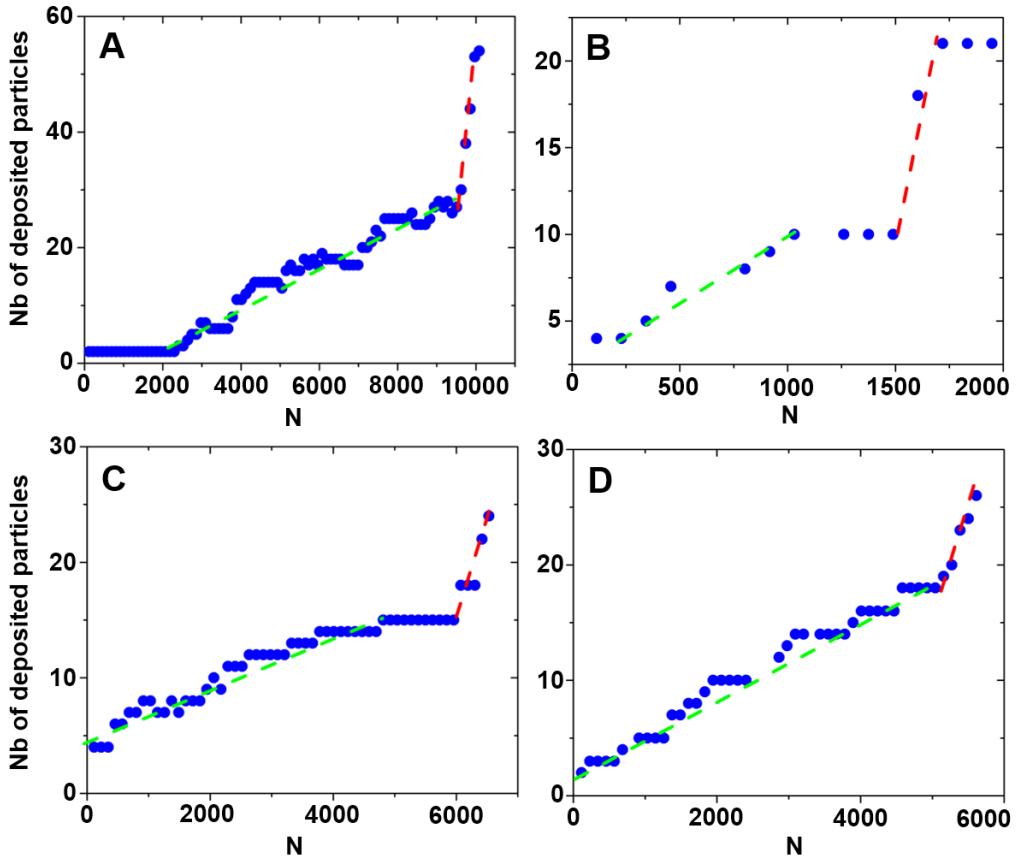


Figure 8: (Top) Dynamics of particle capture for four different pores. Experiments were performed within a *W*=16µm and *H*=12µm channel with 4µm particles at a volume fraction equal to 5.10^{-5} and *ΔP*=30mbar. The green and red dashed lines correspond to linear fits of the data in the first and the second step, respectively. Different views of the clog structure at the end of each of these experiments are provided in Figure 7 (bottom part). In the two figures (7 and 8) the same label corresponds to the same experiment.

2-Mechanisms of particle capture

A-Direct capture

The first deposition mechanism that shows up at the very beginning of pore clogging is the physical interception of particles by the pore walls which we call here "direct capture" as in ref. [10]. Such direct capture events can be observed in images 1 and 2 in Figure 7. This deposition mode relies only on particle capture by the pore surface and thus there is no influence of the particles already deposited within the pore. In our experiments we suppose that there is a direct capture of a particle when it deposits at a distance greater than 1.5*D*, surface to surface, from an immobile particle already inside the pore. Indeed once a particle gets immobilized it modifies the flow around it over a distance we estimate to be around 1.5D from its surface [31]. However here we do not provide any hydrodynamic treatment of the clogging process but instead we give simple rules for the building up of a clog (Figure 10).

Accepted manu

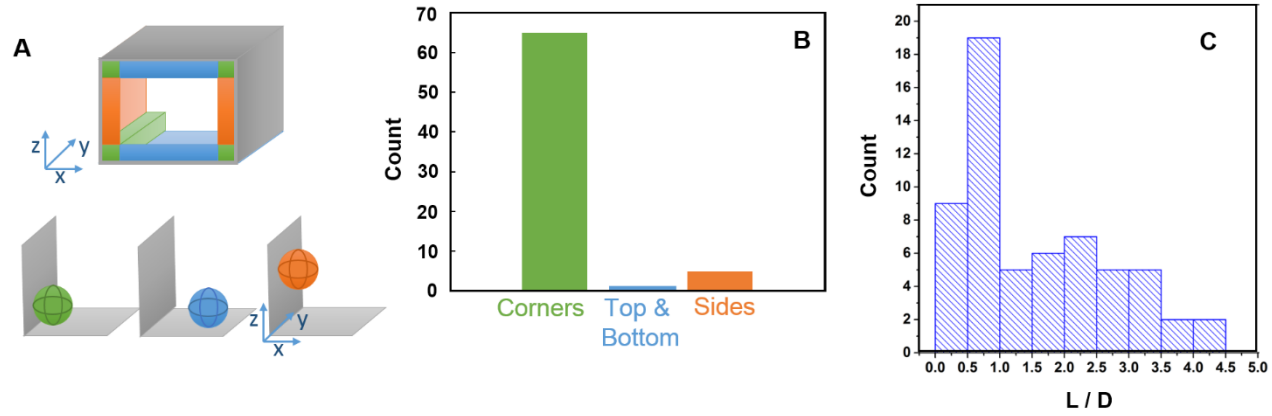


Figure 9: A-Scheme of the three different zones of particle direct deposition onto the walls of the pore. Particles can deposit on corners (green area), horizontal plates (blue areas) or on side walls. (orange area). B-Proportion of the captured particles in each of these zones. C-Distribution of the positions of the particles captured directly by the pore walls from the pore entrance L, scaled by the particle diameter D.

Confocal imaging allows us to determine precisely the distance from the pore entrance, L, at which the first particles get captured directly by the pore wall, and on which wall(s) the particle sticks to (Figure 9A). Most particles get captured at the beginning of the flat part of the pore entrance, just after the curved lip (Figure 1C), at a distance smaller than one particle diameter (peak in Figure 9C). However, we observed that particles can deposit further downstream inside the pore with the capture zone spreading over a distance equal to 4.5D from the pore entrance (Figure 9C). The mean deposition length for direct capture, L , is quantitatively comparable to that we have found in a quasi-2d case [10]. However, the distinctive cross-sectional geometry leads to a different deposition pattern. Deposition events in the direct capture mode are unevenly distributed between corners, side and horizontal walls (Figure 9A). The vast majority of the particles are stuck in the corners (Figure 9A-B). Only a few particles are captured by one of the side walls and almost no particle deposition occurs on the bottom and top walls. This particular spatial arrangement of the particles is due to the pore geometry, to the asymmetry between horizontal and vertical walls. Indeed, lateral sides of the channel present a curved configuration between the reservoir and the pore entrance, while the top and the bottom horizontal ones are flat. Since a local curvature is needed to bend the streamlines, the direct particle capture by physical interception thus expectedly takes place predominantly on lateral walls compared to horizontal walls [4,5,10]. In addition, corners are also particular places with respect to local hydrodynamics, as the flow is much slower, and to particle adhesion, twice as strong in the corners than on a single wall due to the bonding on two pore surfaces instead of one. The probability related to this direct capture mechanism irrespective of the position inside the pore is around 10^{-3}.

B-Indirect capture

We now show, with the help of an example, that quite rapidly during the fouling process most of the particles cannot deposit using the direct capture mode. Here we consider only a given cross section of the pore. As mentioned above direct particle capture occurs mainly in the pore corners. Once a particle gets located in that place, it modifies the flow field around it (grey zone in Figure 10A with a diameter equal to 2.5D). This means that at the moment any incident particle enters partially or completely in the grey zone, its trajectory

Accepted manuscript

ACCEPTED MANUSCRIPT

will be modified by the immobile particle in the corner. In practice more than half of the particles that flow through the cross section will interact hydrodynamically with this immobile one.

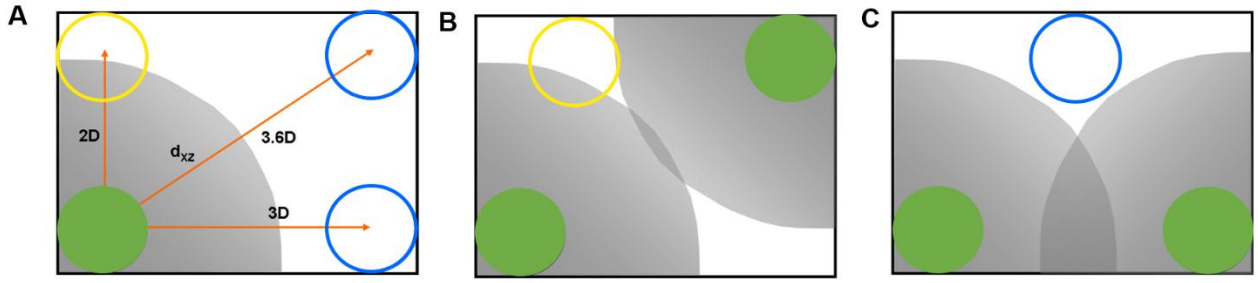


Figure 10: A-Cross section of a pore when a particle is captured in one corner (green). The grey quarter of circle, with a radius equal to 2.5*D*, corresponds to the range of hydrodynamic interaction (HI) created by the captured particle. Top and bottom right corners are the only eligible corners for direct capture positions (blue circles). A particle in the top left corner (yellow circle) would experience HI from the captured one, as would all incident particles within the grey zone, and would have their trajectory modified. B and C-Hydrodynamic influence of two particles captured on corners on opposite sides of the pore. We clearly see that it is only when both captured particles are on the same horizontal wall that incident particles can flow through the pore without experiencing HI from the already captured particles.

This has also a strong impact on where direct capture can occur once a particle is deposited. For instance, direct capture of two particles is impossible on the same lateral side of the pore, since the channel height is only equal to 3*D* (Figure 10A). Therefore, a second direct capture is only possible on opposite lateral sides, as illustrated in Figure 10B-C. Then almost any incident particle will experience hydrodynamic interactions from the deposited ones and will therefore have its trajectory modified. The only configuration allowing a third direct capture is when the first two are both on the same horizontal wall, either the roof or the floor as in Figure 10C. This example is qualitative but it clearly shows that from the very beginning of the experiment, after the deposition of two particles in a given cross-sectional plane, the vast majority of the particle captures will be indirect, i.e., involve hydrodynamic interactions (HI) with static particles. Therefore, directly-captured particles act as sort of 'nucleation nodes' from which further particle accumulation takes place. In the following we focus on the consequences of these HI on the particle capture mechanism.

Accepted manuscript

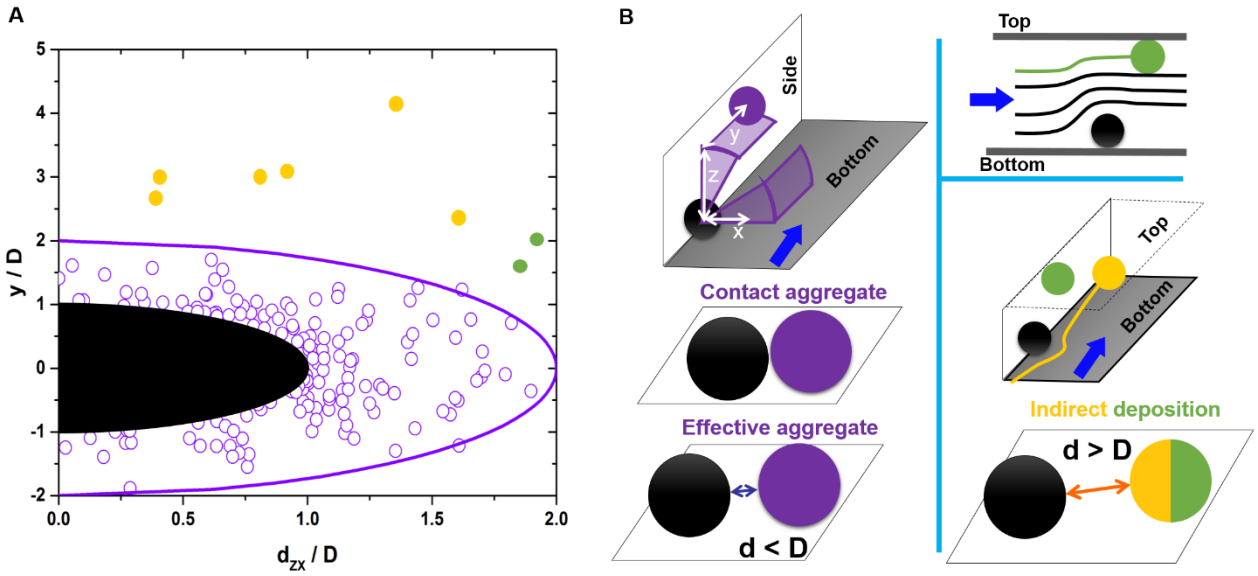


Figure 11: A-Distance of deposition downstream from the static particle in the flow direction (*y*) vs. the distance in *zx* plane, perpendicular to the flow. The black area is the location of the particle already attached on the pore walls. The area delimited by the purple circle corresponds to the aggregation zone where final distances *d* between the two particles, in both planes (*zx* and *zy*), are smaller than *D*. Some particles will deposit further away from the static particle (yellow and green points).
B-Characteristics of the deposition of a newly captured particle (purple, yellow or green particles) on to the pore walls after its interaction with the closest particle already deposited on the pore surface (the black particle). Purple particles are captured at a distance smaller than *D*, forming either a true (contact) or an effective aggregate. Some particles will deposit further away from the static particle (yellow and green). Yellow ones correspond to particles being deposited after crossing an immobile particle but at a distance greater than *D* (middle scheme on the right). Green particles get attached on the same lateral side and the opposite corner (top right corner scheme). Such particles experience a local constriction along the channel height due to the immobile particle in the opposite corner.

Accepted manuscript

We report in Figure 11A the distance between a new deposited particle and the closest immobile one in the pore for the overall building-up of the clog, irrespective of the position of the immobile particle on the pore surface. We define two categories of deposited particles with respect to the surface to surface interparticle distance *d* (Figure 11B). If the new deposited particle gets in contact ($d \approx 0$) with the immobile one, they form a "true" aggregate. As long as *d* is smaller than *D*, they can be considered as forming an "effective" aggregate in the sense that no other particle can be captured thereafter between them. True and effective aggregates correspond to the purple particles in Figure 11. Particles may also be captured at a distance greater than *D* to their closest neighbor, having nonetheless experienced its HI (yellow and green full circles in Figure 11). We observed that newly captured particles quasi-systematically lie in the vicinity of other still ones, at a distance smaller than a particle diameter (inside the purple circle in Figure 11A). Indeed, in all our experiments, only 8 particles out of a total of 170 captured, were deposited at a distance greater than *D* (yellow and green particles in Figure 11A). We thus conclude that, even though we deal with colloidal particles, they cannot have a stable position under flow if they have only one contact with the surface. Most of the time particles with more than two contacts, with either particles or pore walls, do not move once they get captured. In contrast, we observed that few particles that have only one contact may detach from the surface, or they roll very slowly on the surface, typically at few tenth of a micron per minute. Since here we

ACCEPTED MANUSCRIPT

image successively several pores we cannot capture properly these slow rolling motions. We are also unable to observe in real time the particle detachment since it requires the use of a high speed camera [10], typically operating at several thousand frames per second. Nonetheless, it is worth mentioning that these slow rolling motions were rarely observed and we therefore assume they do not influence the clogging scenario significantly. They actually seem more frequent in quasi-2d pores [10]. Few particles (yellow ones) can be deposited up to *4D* downstream from the immobile particle (Figure 11A). They undergo indirect deposition without forming an aggregate and are captured on the sides of the pore but not on the corners (yellow circles in Figure 11B, right side and middle panel). They can also be captured as a result of some imperfections of the pore surface, as mentioned in the previous section. More experiments are needed to characterize this specific indirect deposition mode. Finally, a particle stuck in a corner can also create two local asymmetric constrictions, one on each of the sides which this particle is in contact with. As a result some of the fluid streamlines around the static particle (black full circle) are deviated towards the walls (scheme in the top right corner of Figure 11B). When a particle (green one) flows in the vicinity of the immobile particle it will follow one of these streamlines, move towards the opposite wall where it can eventually get captured. To sum up, with the help of a simple criterion based on the distance *d* between particle surfaces, defined in Figure 11, we can divide all the particles deposited on the pore walls after the very first ones (direct capture) into three categories, indirect, effective or contact aggregates.

We have also determined the coordination number, i.e., the number of neighbors that are in true contact with a given particle, of all the particles belonging to this first layer. Note that this coordination number include the contact between the particle and the pore surface. We report in Figure 12A the distribution of coordination numbers, showing the relative contribution of the three categories defined above. Only 3% of the total number of particles, a population that corresponds to indirect deposition, were isolated at the time they get captured. These are in contact only with one of the lateral sides. All the other particles (97%) participate in an aggregate, either true or effective: 34% form true (contact) aggregates, while the remaining 63% form effective aggregates in contact with one or two particles. Therefore, it seems that particle capture in the close vicinity of another one, or near an aggregate, favors the subsequent capture of other flowing individuals.

It is also worth noting that particles captured by aggregates generally deposit downstream. In this way, the first layer of particles progressively invades the pore, from its entrance, as shown in Figures 8 and 13. We have plotted in Figure 12B the distribution of the deposition length from the pore entrance for all the particles that have undergone an indirect capture. We clearly see that although most of the particles are located in close proximity of the pore entrance, i.e., for L/D <3, some of them deposit further downstream up to L/D=7 in the flow direction during the progressive growth of the fouling layer. This means that the reduction of the pore cross section due to particle accumulation should be mostly reduced near the pore entrance, for L/D <3, leading to the final obstruction of the pore there. This is confirmed in the four examples of pores clogged in Figure 7 (bottom).

Accepted manuscript

ACCEPTED MANUSCRIPT

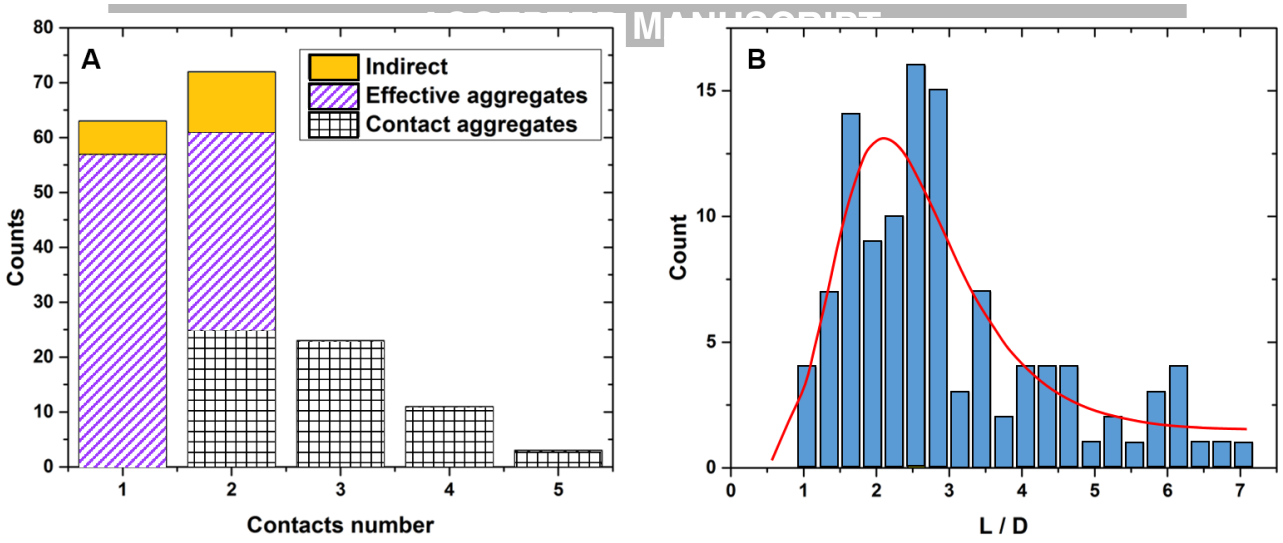


Figure 12: A-Distribution of the number of contacts for the particles belonging to the first layer in all the considered pores. The definition of each category is in figure 11B. These numbers do not include the contact with the pore surface. B- Distribution of the deposition lengths from the pore entrance for particles having interacted with a deposited particle or an aggregate. The (red) line is a log-normal fit of the data peaked around 2.1 *L/D*.

C-Second layer

As the pore gets partially clogged by the first layer, particles start depositing on this layer and therefore have no contact with the pore surface. Four examples are shown in Figure 13A. The four sides of the pore do not have to be fully covered for this second layer deposition to start. From the examples in Figure 13 we can see that particles do not get stuck where the cross section is the narrowest but can be captured anywhere within the pore. As soon as two to three particles cover the pore surface locally, in such a way that no other particle can be lodged within the remaining place on the pore surface, between them, then a particle may deposit on top of the other individuals. We also measured the number of contacts of these second-layer particles (Figure 13B). The contact number is between one and four. Contrary to the first layer 35% of the particles are in contact with only one neighbor. We do not know if those particles remain permanently in contact or if later on they are detached by the flow; the particle deposition is quite fast at the end of the clogging process and does not allow us to monitor such dynamics. Indeed, several particles get captured at the same time and we cannot track the position of each particle unambiguously.

Accepted manuscript

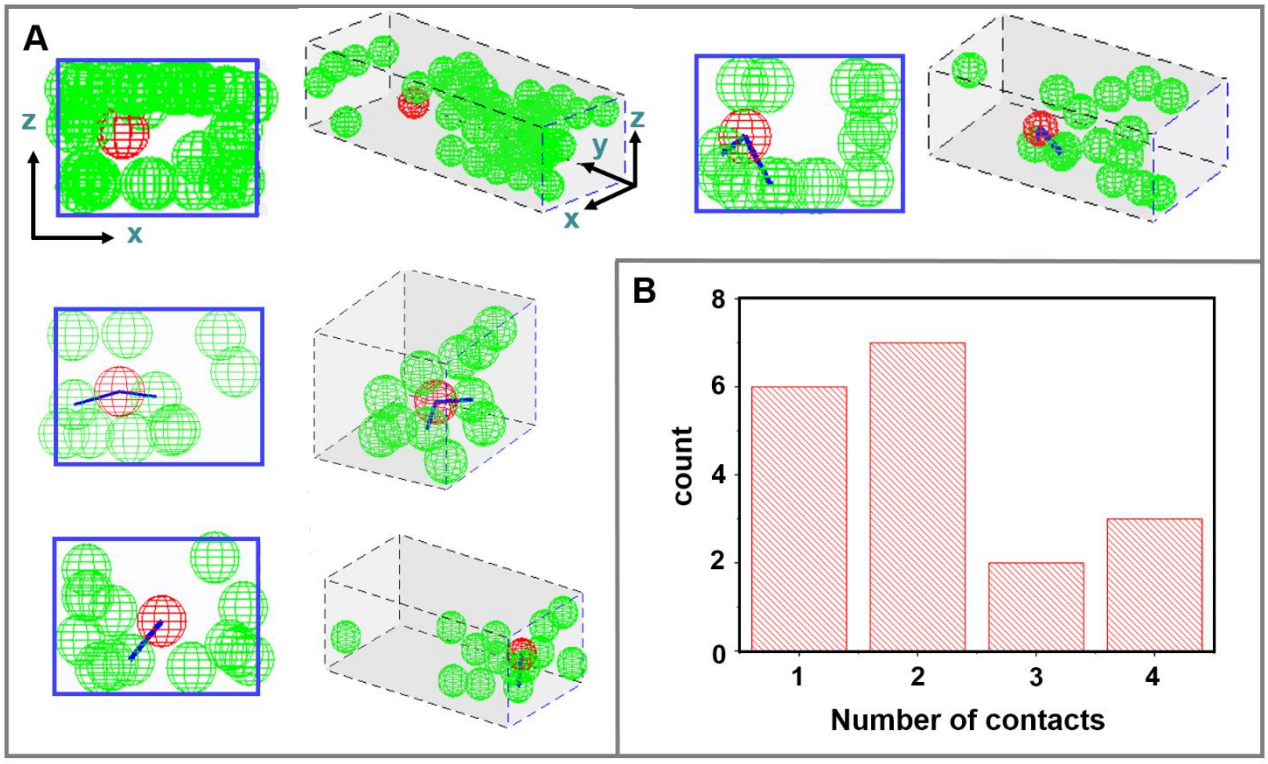


Figure 13: A-Partial fouling of four pores at the moment when the deposition on the second layer starts (red sphere). The green particles are those belonging to the first layer, in contact with the pore walls. The blue lines connecting red and green particles correspond to the direct contacts of this particle with its first layer neighbor. For each experiment, we have represented a projection of all particles in a cross–sectional view (left), and a 3d view of the partial clog (right) in which the flow goes from the right to left. B-Distribution of the coordination numbers of particles deposited in the second layer.

3-Colloidal aggregate growth: toward complete pore clogging

Figures 11 and 12 show that the progressive clogging of the pore corresponds to the growth of aggregates since almost all the particles that are captured within the pore deposit near already captured particles. Overall, static particles within the pore act as "attractors" for the others which flow in their vicinity. We identified the different aggregates and characterized their individual growth over time. In each of the clogged pores we studied, there are two to four aggregates, at most, that grow at the same time and rapidly merge as they clog the pore. A typical clog formation is shown in Figure 14, which corresponds to the deposition curve shown in Figure 8B. The particles are color-coded according to the aggregate they belong to; isolated particles are represented in blue. At the beginning of the pore filling (image 1), two isolated particles are deposited on the right lateral wall while a first aggregate forms on the opposite wall (purple particles). The aggregate grows (image 2) until it catches one of the isolated particles (image 3). As a direct illustration of the role of aggregates mentioned above, most of the newly captured particles participate in the growth of this aggregate during the build-up of the clog. In parallel, a second aggregate (pink particles) also starts to grow (image 4), as a result of the capture of a flowing particle in the vicinity of the remaining isolated particle, deposited right at the beginning of the experiment. The first aggregate, as it grows, ends up merging with this second aggregate (image 5). This growth also favors the deposition of particles on top of the first particle

Accepted manuscript

ACCEPTED MANUSCRIPT

layer. The capture rate thus starts increasing as observed in Figure 8B, as the main (and now sole) aggregate spreads all over the pore cross section and thereby increasingly obstructs to the incident particles (image 6).

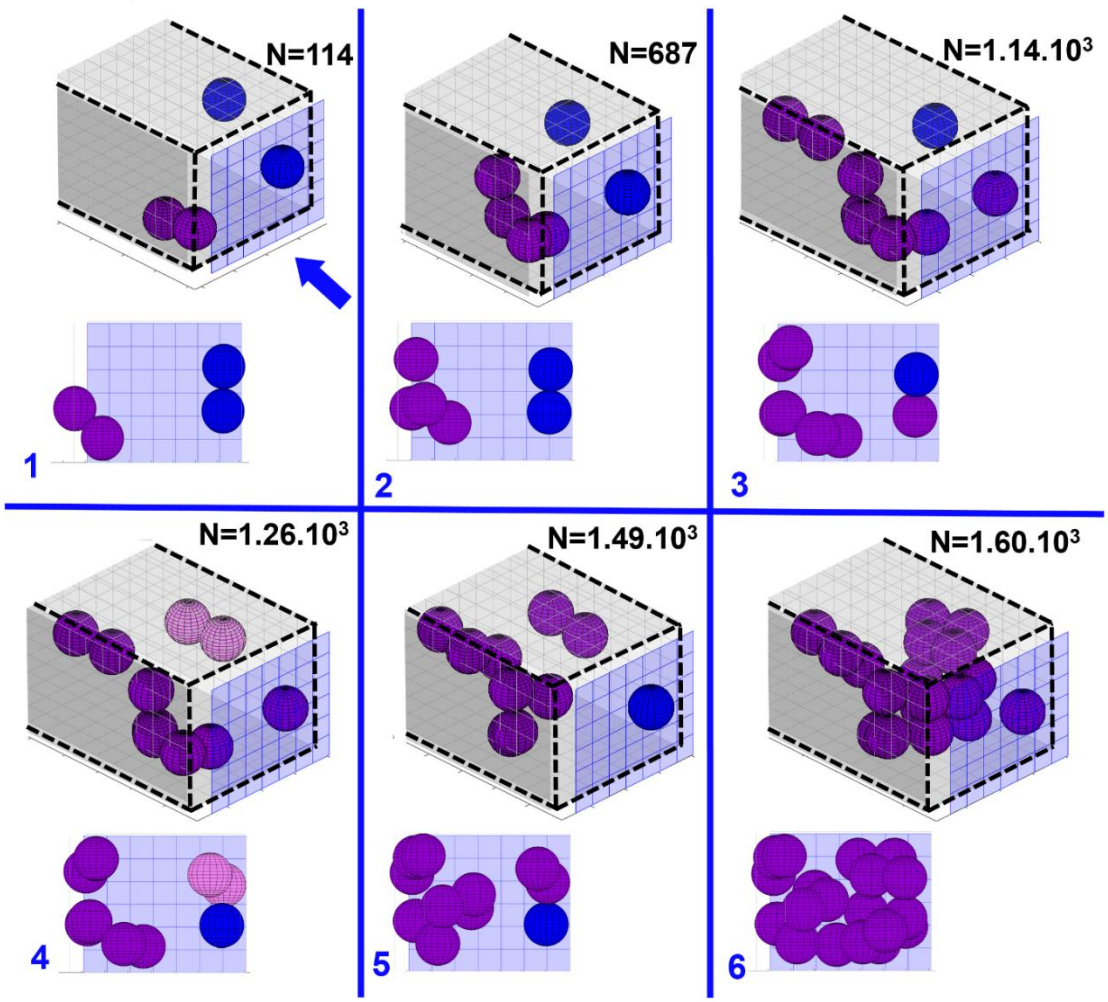


Figure 14: 3D images of the clog buildup corresponding to the deposition curve in Figure 8B. In each image, blue particles are isolated, while pink and purples ones belong to two different aggregates. The arrow indicates the flow direction.

Discussion

In this work we investigate the fouling process at the particle level within a model filter. We focus on an intermediate degree of confinement *W/D* for which, in principle, very few particles are required to block the pore [4]. In this approach, a particle gets captured and then reduces locally the cross section of the pore, which in turn increases the probability to capture another particle at the same place, thereby further reducing the cross section. Following this deposition process, only between seven and twelve particles would be needed to block a given section of the pore. Here we have observed that the actual number of particles needed is in fact in the range of 20-50 (Figure 8) because the particle deposition spreads along the pore, which obviously requires more objects than if the capture occurred in a single cross-sectional plane. Figure 8 also shows that the successive captures do not modify the kinetics of pore fouling in a given regime, which means that the local reduction of the cross section does not result in an increase of particle capture.

ACCEPTED MANUSCRIPT

Surprisingly we decorate progressively the pore walls with a constant deposition rate. This means that the increase (decrease) of the hydrodynamic resistance (average flow rate) of the partially fouled pore does not impact the capture probability. We showed that this type of fouling relies on aggregates growth. From almost the very beginning of the deposition process, particles predominantly get captured really close to ($d < D$), if not in contact of, those already captured. These aggregates first grow on the pore surface, mostly along the flow direction. This growth corresponds to the first step of the pore-scale deposition dynamics (Figure 8). Later aggregates also grow toward the pore center, i.e., particles deposit on top of each other, which manifests at the pore scale by a faster deposition dynamics (second step). Note that during this second step the aggregate also keeps growing along the pore surface (Figure 14, images 5 and 6).

The particle deposition process is related to the particle and pore surface properties, i.e., the DLVO interaction potentials between particles and the pore surface. When using PS particles (life Technology) with a lower surface charge (zeta potential equal to -35 mV) and a stronger van der Waals attraction compared to the PMMA considered here, we observed quantitatively different deposition patterns [5]. Here pore blocking still relies on the growth of few aggregates that eventually merge and completely obstruct the pore, the aggregates spread much less on the pore surface before merging with other aggregates and blocking the pore. The length of the first layer of particles in contact with the pore surface is roughly equal to 1.4W, while it is closer to 2.5W with PMMA particles, for similar degrees of confinement and deposition regimes. In addition the average number of particles that have to pass through the pore prior clogging is three orders of magnitude higher for PMMA particles compared to PS ones; increasing the salinity of the suspension significantly reduces this number. Intuitively, particles with a lower surface charge and/or a stronger adhesion form clogs more rapidly as the aggregates are more stable [28], and fewer particles are required to block the pore. However, from these experiments with PS and PMMA particles we cannot determine respectively the influence of each part of the DLVO potential. We conjecture that, on the one hand, the high surface charge of PMMA particles favors 2d aggregation along the PDMS pore surface, which is far less charged [32], rather than on already deposited particles. On the other hand, the weak interparticle and particle-pore van der Waals attractions globally reduces the stable particle deposition. This weaker adhesion compared to PS is even more reduced by the nearly refractive index matching that is required to image the structure of the clog at the particle level [33]. At the very beginning of the pore clogging the vast majority of the particles are captured in pore corners (Figure 9a-c), where the adhesion is the strongest since particles are in contact with two pore surfaces, and where the flow intensity is the lowest. Some particles may be captured temporarily in other parts of the pore (lateral, top and bottom walls, Figure 9c) but the flow rapidly wipes them off the pore surface. We managed to observe such a deposition-release event in Figure 7 where a particle adheres on top of a static particle (red particle in image 4) and is then released (absent in image 5). A static particle on the pore surface can also be detached when a flowing particle passes by in its close vicinity. In a typical experiment, each pore is imaged by the confocal microscope every 30s and between two consecutive image stacks of the same pore, typically a 100 to 500 particles have flowed through it, of which only one or two get captured on average. It thus is reasonable to consider that a greater part of these flowing particles also come closer to the pore walls/aggregates and thus could be as least transiently captured. This fast dynamics of

Accepted manuscript

ACCEPTED MANUSCRIPT

capture and release is not accessible by our imaging technique since these events, which last around 100 µs, would require an imaging system able to acquire images at a frame rate between 5000 and 10000 frames per second [10]. We conclude that 3d imaging with a confocal microscope only records the particles that are the most stable under flow over time, i.e., those which have a sufficiently strong contact interaction with either the pore surface or the other static particles. This remains true throughout the whole clog formation process.

The present work is restricted to only one type of particle, suspending liquid and pore wall, but it would be really valuable to extend the investigation systematically by using a wide range of DLVO parameters and coupling them with different flow conditions. Undoubtedly the monitoring of the progressive clog formation at the particle level could be done with many other types of colloidal particles commonly used in industry (ie silica, $CaCO_3$, microgels[6], protein aggregates….) as long as we use a fluorescent dye within these particles and have a slight mismatch between the refractive index of the particles and that of the suspending liquid, allowing the use of confocal imaging. In the present study this mismatch is around 0.06 and this value allows us to determine precisely the position of particle center for a maximum seven particles up to a layer of 3 particles thick. In stronger confinement conditions (lower ratio *W/D*), with a pore height not greater than three particle layers, slightly higher refractive index mismatches could still allow the quantitative imaging of other types of colloids.

Recently, advanced simulations have tackled the issue of clogging at the pore scale [31,34–36]. Even though they take a great care of the hydrodynamics of particle capture as well as the DLVO forces, they do not feature deposition patterns similar to those observed in this work. Even in the simplest case restricted to particle deposition on the pore surface, these numerical works neither provide an accurate deposition rates nor realistic spatial positioning of the particles on the surface. For example Abgangla et al. [31] and Trofa et. al.[36] need to "clue" particles on the pore surface, making sure that there is a uniform spatial distribution of the particles all along the pore surface, before running their pore clogging simulations. Very recently, Lohaus et al. [34] used a coupled CFD-DEM with a more accurate description of the DLVO forces but they neglected the particle capture on top and bottom walls, focusing only on the laterals walls. The particle volume fraction they obtained on the laterals walls, corresponding to the random close packing of particles, thus seems excessively high compared to our experiments. This difference is however not totally surprising since they also used different flow conditions and DLVO parameters. Interestingly, Trofa et. al.[36] included the coupling between the aggregate growth from a pore wall and the fluid around it, which is able to break some parts of the growing aggregate. They observed that large fragments of the aggregates, which involve tens of particles, can be detached by the flow. In contrast, in our experiments, where the adhesion of a particle either with the wall or with other particles is rather weak and where the shear rate is greater than in this numerical study, only one particle at a time can be detached from the growing aggregate, and such event remains rare (Figures 7 and 8). This suggests that the choice of the adhesion condition between particles in numerical simulations has a dramatic impact on the aggregate growth, as was actually pointed out by Trofa et al.[36]. In the future extensive numerical studies of a single pore clogging by colloidal particles should be performed by varying systematically the parameters of colloidal interaction potentials (particle-particle and the particle-wall) to better elucidate this influence. These results then have to be compared to experimental

Accepted manuscript

ACCEPTED MANUSCRIPT

work done under the exact same conditions, for which we are now able to provide the structural features of the fouling layers at the particle level, following the methodology proposed in this paper.

In a more general point of view, we showed that using a devoted setup and advanced image analysis greatly helps to understand structural aspects of the fouling of model membranes (microfluidic channels or microsieves), and even industrial membranes. To this end, one needs to ensure a reasonably small index mismatch between the fluid, the membrane and the particles. In such conditions, Skaug and Schwartz [37,38] determined the dynamics of 40nm PS nanoparticles within a membrane of glass fiber and nitrocellulose. Following this strategy we may also locate where the fouling takes place, i.e. at the top or within the pore of a given membrane. In the same vein, we may also look at the early formation of the cake on top of a membrane, either in dead-end or in cross-flow conditions, corresponding to the accumulation of several layers of particles. As we have shown in this work we can image, in principle, through these layers and determine the structure and the local permeability of the cake in various flow and physico-chemical conditions. More importantly, the stability under flow of this cake can be investigated, in order to assess the membrane cleaning process by back wash for instance. It is indeed rather easy to increase gradually the flow rate in order to wipe off some particles or aggregates on top of the cake. For all the imposed flow conditions we could thus effectively determine at the particle level how the cake is eroded by the flow and the size distribution of the detached aggregates.

Conclusion

We carried out experimental studies of the fouling process within a single pore by colloidal particles using a high speed confocal microscope. Thanks to this technique we determined for the first time the different steps of the progressive fouling process at the pore and at the particle scales. At the very beginning of the process, isolated particles are captured by the pore walls at the pore corners, which are the most stable places against flow. Quite rapidly the deposition of new particles is strongly conditioned by those that are already deposited. Particles get captured quasi-systematically near an immobile one or near an aggregate. We observed that only 2-4 isolated aggregates form inside the pore, which first grow independently, and thereafter merge. Due to the high surface charge of the colloidal particles these aggregates first grow along the flow direction before also growing towards the pore center which eventually block the pore completely. Beyond this basic scenario, more work is needed to understand the general aggregation processes of colloidal particles in confined environments. The methodology we developed, based on confocal imaging of fluorescent particles and image analysis to get the precise position of individual particles as the pore gets progressively fouled, could in principle be generalized to investigate in a systematic way the membrane clogging by various types of colloidal particles within the limit of high confinement. These experiments could also be used as a benchmark for theoretical and numerical modeling of the different physical processes at play in the fouling process.

Accepted manuscript

ACCEPTED MANUSCRIPT

Acknowledgements

We acknowledge the French Agence Nationale de la Recherche (ANR) (ANR-12-JS09-0003) and the CNES (Collmat) for their funding support.

References

[1] E. Dressaire, A. Sauret, Clogging of microfluidic systems, Soft Matter. (2016). doi:10.1039/C6SM01879C.
[2] X. Chen, J. Shen, Z. Hu, X. Huo, Manufacturing methods and applications of membranes in microfluidics, Biomed. Microdevices. 18 (2016) 104. doi:10.1007/s10544-016-0130-7.
[3] P. Bacchin, A. Marty, P. Duru, M. Meireles, P. Aimar, Colloidal surface interactions and membrane fouling: investigations at pore scale, Adv. Colloid Interface Sci. 164 (2011) 2–11.
[4] H.M. Wyss, D.L. Blair, J.F. Morris, H.A. Stone, D.A. Weitz, Mechanism for clogging of microchannels, Phys. Rev. E. 74 (2006) 061402.
[5] B. Dersoir, M.R. de S. Vincent, M. Abkarian, H. Tabuteau, Clogging of a single pore by colloidal particles, Microfluid. Nanofluidics. 19 (2015) 953–961. doi:10.1007/s10404-015-1624-y.
[6] J. Linkhorst, T. Beckmann, D. Go, A.J.C. Kuehne, M. Wessling, Microfluidic colloid filtration, Sci. Rep. 6 (2016) 22376. doi:10.1038/srep22376.
[7] F. Tian, J. Lyu, J. Shi, F. Tan, M. Yang, A polymeric microfluidic device integrated with nanoporous alumina membranes for simultaneous detection of multiple foodborne pathogens, Sens. Actuators B Chem. 225 (2016) 312–318. doi:10.1016/j.snb.2015.11.059.
[8] D.C. Duffy, J.C. McDonald, O.J.A. Schueller, G.M. Whitesides, Rapid Prototyping of Microfluidic Systems in Poly(dimethylsiloxane), Anal. Chem. 70 (1998) 4974–4984. doi:10.1021/ac980656z.
[9] Z.B. Sendekie, A. Gaveau, R.G. Lammertink, P. Bacchin, Bacteria Delay the Jamming of Particles at Microchannel Bottlenecks, Sci. Rep. 6 (2016). https://www.ncbi.nlm.nih.gov/pmc/articles/PMC4980593/ (accessed November 16, 2016).
[10] B. Dersoir, A. B. Schofield, H. Tabuteau, Clogging transition induced by self filtration in a slit pore, Soft Matter. 13 (2017) 2054–2066. doi:10.1039/C6SM02605B.
[11] S.S. Massenburg, E. Amstad, D.A. Weitz, Clogging in parallelized tapered microfluidic channels, Microfluid. Nanofluidics. 20 (2016) 94. doi:10.1007/s10404-016-1758-6.
[12] A. Sauret, E.C. Barney, A. Perro, E. Villermaux, H.A. Stone, E. Dressaire, Clogging by sieving in microchannels: Application to the detection of contaminants in colloidal suspensions, Appl. Phys. Lett. 105 (2014) 074101.
[13] B. Mustin, B. Stoeber, Deposition of particles from polydisperse suspensions in microfluidic systems, Microfluid. Nanofluidics. 9 (2010) 905–913.
[14] Z.B. Sendekie, P. Bacchin, Colloidal Jamming Dynamics in Microchannel Bottlenecks, Langmuir. 32 (2016) 1478–1488.
[15] T. van de Laar, S. ten Klooster, K. Schroën, J. Sprakel, Transition-state theory predicts clogging at the microscale, Sci. Rep. 6 (2016) 28450. doi:10.1038/srep28450.
[16] R. van Zwieten, T. van de Laar, J. Sprakel, K. Schroën, From cooperative to uncorrelated clogging in cross-flow microfluidic membranes, Sci. Rep. 8 (2018) 5687. doi:10.1038/s41598-018-24088-6.
[17] G. Brans, A. van Dinther, B. Odum, C.G.P.H. Schroën, R.M. Boom, Transmission and fractionation of micro-sized particle suspensions, J. Membr. Sci. 290 (2007) 230–240. doi:10.1016/j.memsci.2006.12.045.
[18] M.E. Warkiani, F. Wicaksana, A.G. Fane, H.-Q. Gong, Investigation of membrane fouling at the microscale using isopore filters, Microfluid. Nanofluidics. 19 (2015) 307–315. doi:10.1007/s10404-014-1538-0.
[19] I.S. Ngene, R.G.H. Lammertink, M. Wessling, W. van der Meer, A microfluidic membrane chip for in situ fouling characterization, J. Membr. Sci. 346 (2010) 202–207. doi:10.1016/j.memsci.2009.09.035.

Accepted manuscript

ACCEPTED MANUSCRIPT

[20] I.S. Ngene, R.G.H. Lammertink, M. Wessling, W.G.J. Van der Meer, Visual characterization of fouling with bidisperse solution, J. Membr. Sci. 368 (2011) 110–115. doi:10.1016/j.memsci.2010.11.026.
[21] R.L. Hartman, J.R. Naber, N. Zaborenko, S.L. Buchwald, K.F. Jensen, Overcoming the challenges of solid bridging and constriction during Pd-Catalyzed C- N bond formation in microreactors, Org. Process Res. Dev. 14 (2010) 1347–1357.
[22] L. Sicignano, G. Tomaiuolo, A. Perazzo, S.P. Nolan, P.L. Maffettone, S. Guido, The effect of shear flow on microreactor clogging, Chem. Eng. J. 341 (2018) 639–647. doi:10.1016/j.cej.2018.02.037.
[23] R.L. Hartman, Managing Solids in Microreactors for the Upstream Continuous Processing of Fine Chemicals, Org. Process Res. Dev. 16 (2012) 870–887. doi:10.1021/op200348t.
[24] S. Shen, E.D. Sudol, M.S. El-Aasser, Control of particle size in dispersion polymerization of methyl methacrylate, J. Polym. Sci. Part Polym. Chem. 31 (1993) 1393–1402. doi:10.1002/pola.1993.080310606.
[25] T.M. Squires, S.R. Quake, Microfluidics: Fluid physics at the nanoliter scale, Rev. Mod. Phys. 77 (2005) 977.
[26] J.C. Crocker, D.G. Grier, Methods of Digital Video Microscopy for Colloidal Studies, J. Colloid Interface Sci. 179 (1996) 298–310. doi:10.1006/jcis.1996.0217.
[27] M.C. Jenkins, S.U. Egelhaaf, Confocal microscopy of colloidal particles: Towards reliable, optimum coordinates, Adv. Colloid Interface Sci. 136 (2008) 65–92. doi:10.1016/j.cis.2007.07.006.
[28] M.R. de Saint Vincent, M. Abkarian, H. Tabuteau, Dynamics of colloid accumulation under flow over porous obstacles, Soft Matter. 12 (2016) 1041–1050.
[29] T. Dabroś, T.G.M. van de Ven, Surface collisions in a viscous fluid, J. Colloid Interface Sci. 149 (1992) 493–505. doi:10.1016/0021-9797(92)90436-P.
[30] V. Ramachandran, H.S. Fogler, Multilayer deposition of stable colloidal particles during flow within cylindrical pores, Langmuir. 14 (1998) 4435–4444.
[31] G.C. Agbangla, E. Climent, P. Bacchin, Numerical investigation of channel blockage by flowing microparticles, Comput. Fluids. 94 (2014) 69–83.
[32] B. Mustin, B. Stoeber, Single Layer Deposition of Polystyrene Particles onto Planar Polydimethylsiloxane Substrates, Langmuir. 32 (2016) 88–101. doi:10.1021/acs.langmuir.5b02914.
[33] W.C. K. Poon, E. R. Weeks, C. Patrick Royall, On measuring colloidal volume fractions, Soft Matter. 8 (2012) 21–30. doi:10.1039/C1SM06083J.
[34] J. Lohaus, Y.M. Perez, M. Wessling, What are the microscopic events of colloidal membrane fouling?, J. Membr. Sci. 553 (2018) 90–98. doi:10.1016/j.memsci.2018.02.023.
[35] P. Bacchin, Q. Derekx, D. Veyret, K. Glucina, P. Moulin, Clogging of microporous channels networks: role of connectivity and tortuosity, Microfluid. Nanofluidics. 17 (2014) 85–96.
[36] M. Trofa, G. D'Avino, L. Sicignano, G. Tomaiuolo, F. Greco, P.L. Maffettone, S. Guido, CFD-DEM simulations of particulate fouling in microchannels, Chem. Eng. J. 358 (2019) 91–100. doi:10.1016/j.cej.2018.09.207.
[37] M.J. Skaug, L. Wang, Y. Ding, D.K. Schwartz, Hindered Nanoparticle Diffusion and Void Accessibility in a Three-Dimensional Porous Medium, ACS Nano. 9 (2015) 2148–2156. doi:10.1021/acsnano.5b00019.
[38] M.J. Skaug, D.K. Schwartz, Tracking Nanoparticle Diffusion in Porous Filtration Media, Ind. Eng. Chem. Res. 54 (2015) 4414–4419. doi:10.1021/ie503895b.

Accepted manuscript

ACCEPTED MANUSCRIPT

Highlights

1- Experimental works to determine the colloidal fouling of a single pore at the particle scale
2- Quantifying particle deposition rate and fouling dynamics up to the complete pore blocking
3- Determination of the aggregate growth dynamics

Accepted manuscript